JACS
JOURNAL OF THE AMERICAN CHEMICAL SOCIETY
Article
pubs.acs.org/JACS

Formation and Healing of Vacancies in Graphene Chemical Vapor Deposition (CVD) Growth

Lu Wang,[‡] Xiuyun Zhang,[†] Helen L.W. Chan,[‡] Feng Yan,*[,‡] and Feng Ding*[,†]

[†]Institute of Textile and Clothing and [‡]Department of Applied Physics, Hong Kong Polytechnic University, Kowloon, Hong Kong, People's Republic of China

Supporting Information

ABSTRACT: The formation and kinetics of single and double vacancies in graphene chemical vapor deposition (CVD) growth on Cu(111), Ni(111), and Co(0001) surfaces are investigated by the first-principles calculation. It is found that the vacancies in graphene on the metal surfaces are dramatically different from those in free-standing graphene. The interaction between the vacancies and the metal surface and the involvement of a metal atom in the vacancy structure greatly reduce their formation energies and significantly change their diffusion barriers. Furthermore, the kinetic process of forming vacancies and the potential route of their healing during graphene CVD growth on Cu(111) and Ni(111) surfaces are explored. The results indicate that Cu is a better catalyst than Ni for the synthesis of high-quality graphene because the defects in graphene on Cu are formed in a lower concentration and can be more efficiently healed at the typical experimental temperature. This study leads to a deep insight into the atomic process of graphene growth, and the mechanism revealed in this study can be used for the experimental design of high-quality graphene synthesis.

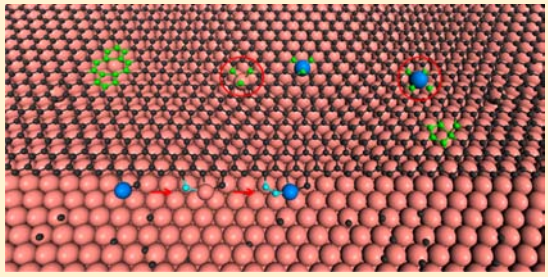

1. INTRODUCTION

Graphene has attracted extensive research interests recently due to its outstanding physical, chemical, and electronic properties and numerous potential applications.[1−3] In particular, the extremely high carrier mobilities in graphene with the theoretical limit of ∼200 000 $cm^2\ V^{-1}\ s^{-1}$ ensure it the best candidate for replacing silicon in the future electronics.[4] Unfortunately, these outstanding properties of graphene may be greatly degraded for the existence of defects in the honeycomb lattice. Thus, the synthesis of high-quality graphene is essential to its practical applications. Among the present technologies of graphene synthesis, the chemical vapor deposition (CVD) method is the most intensively investigated one[5−13] and has been recognized as the most promising approach to achieving this target.

To date, although large-area graphene films have been successfully synthesized by the CVD method, the quality of them is not as good as expected. For example, most of the reported carrier mobilities of CVD graphene are 1000−3000 $cm^2\ V^{-1}\ s^{-1}$,[5,6] which are still about 1 order of magnitude lower than those of the mechanically exfoliated one[14] and 2 orders of magnitude lower than the theoretical limit.[4] The low mobilities have been attributed to the carrier scattering at the grain boundaries (GBs) between single-crystalline domains.[15] Recently, by suppressing the nucleation of graphene or using the seeded growth strategy, the technology of growing graphene with very large single crystalline domains, which sizes up to mm scale, has developed.[13,16] However, the carrier mobilities of the large-domain CVD-grown graphene are only improved to ∼4000 $cm^2\ V^{-1}\ s^{-1}$,[16] which are still much lower than those of the exfoliated graphene, although the CVD-grown one already has larger domain sizes.[17] Therefore, there must be other defects in the CVD samples that scatter or trap carriers. Beyond the linear GBs, various point defects are the most potential candidates which are responsible for the downgrading of graphene's quality. Thus, understanding of the structural stability and formation of point defects during graphene CVD growth and the healing of these point defects are pressing and important to improve graphene's quality by further optimizing the experimental design.

Single and double vacancies (SV and DV) in free-standing graphene[18−22] and the walls of CNTs[23−25] and transition-metal atoms embedded in these vacancies[26−29] have been extensively investigated theoretically. In free-standing graphene, the ground structure of a SV has a pentagon-dangling bond (5-DB) formation.[19,22] Its formation energy is as high as 7.5 eV, but it can diffuse quickly in graphene by overcoming a low diffusion barrier of 1.3 eV.[19,22] The coalescence of two SV directly leads into the formation of pentagon|octagon|pentagon (5|8|5), which is a metastable structure of a DV and can be further reconstructed into the ground structure of the DV, the 555−777 formation.[20] The diffusion barrier of a DV in graphene is ∼7 eV, drastically higher than that of SV and implying the immobility nature of DV.[22] During CVD growth, graphene is formed on a transition-metal surface, and thus any C atom that has a DB around a point defect can be passivated by the catalyst surface, which may lead to great changes in the formation

Received: December 29, 2012
Published: February 27, 2013

   dx.doi.org/10.1021/ja312687a | J. Am. Chem. Soc. 2013, 135, 4476−4482

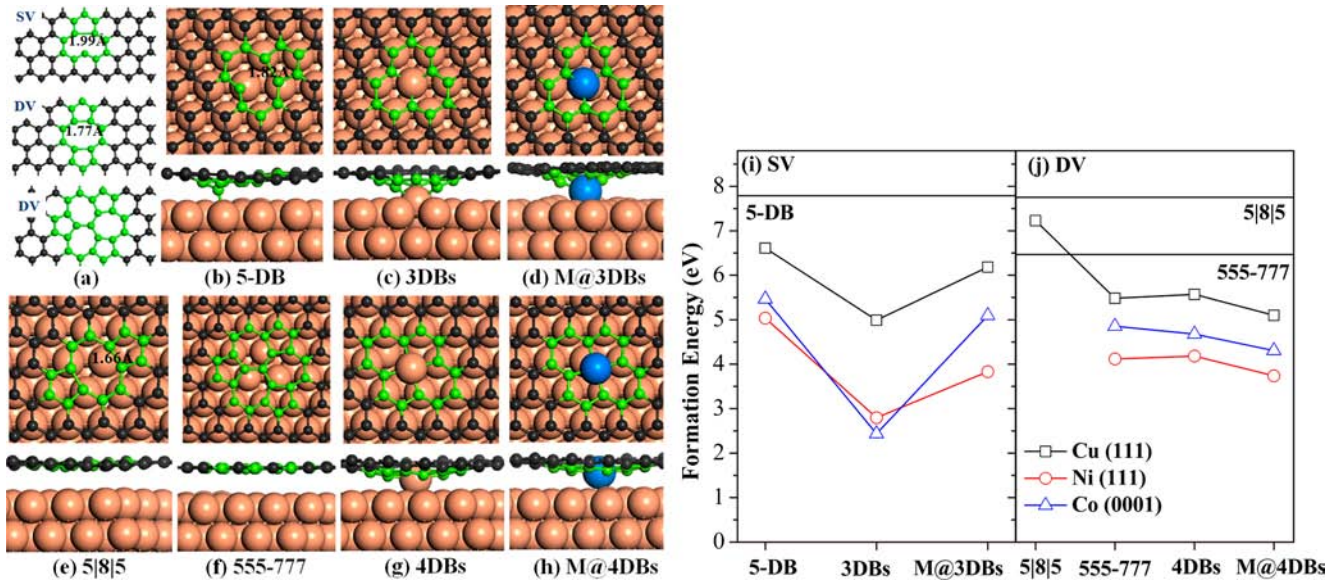

Figure 1. (a) Optimized structures of a SV (5DB) and a DV (5|8|5 and 555−777) in free-standing graphene and (b−d) SV and (e−h) DV in graphene on the Cu surface (top and side views). Carbon atoms around defect and the extra metal adatom in M@3DBs and M@4DBs structures are highlighted by green and blue, respectively. (i,j) The formation energies of SV and DV in graphene on Cu, Ni, and Co surfaces in comparison with those in free-standing graphene (illustrated by black lines).

energies, diffusion barriers, and even the order of stability of competitive structures, such as the 5|8|5 and 555−777 of DV. Therefore, understanding the properties of these point defects in graphene on different catalyst surfaces is very important for the experimental design. In particular, the quality of graphene is expected to be improved by selecting a proper catalyst on which the point defects are less stable and can be efficiently healed during the growth. However, to our best knowledge, there is no systematic theoretical study on this issue, although its importance has been evidenced by a few experiments.[30−32]

In this article, we report a systematic theoretical study on the formation of SV and DV during the CVD growth of graphene on three of the mostly used catalyst surfaces: the (111) surfaces of fcc Cu and Ni and (0001) surface of hcp Co. The structure, formation energy, and mobility of the defects are explored first, and significant difference between the vacancies in free-standing graphene and metal−supported graphene is revealed. The strong interactions between metal and dangling C atoms at the vacancy sites can greatly change the vacancy structures, where the SV tends to have three dangling C atoms bonded to the catalyst surface (3DBs), and the one additional metal atom locating in the center of a DV (M@4DBs) is energetically more preferable than other configurations. The formation energy of a SV is dramatically decreased, and its diffusion barrier is significantly increased to 3.0−4.0 eV due to the strong interaction with the metal surface, which implies the exceptional stability of the SV on metal surfaces. The involvement of a metal atom at the center can greatly stabilize the DV and maintain its high diffusion barrier. Besides, our further exploration on the formation process and healing mechanism of DV in graphene on Cu or Ni surfaces suggests that Cu is a better catalyst than Ni for high-quality graphene synthesis because of the larger defect formation energy and the lower barrier of defect healing on Cu. Therefore, this study provides a guideline for the selection of catalyst and growth temperature in the synthesis of high-quality graphene.

2. MODELING AND COMPUTATIONAL DETAILS

Among the commonly used catalysts for graphene CVD growth, including Rh,[33] Ru,[34] Ni,[35,36] Ir,[37] Pt,[38] Pd,[39] Cu,[40] and Co,[41] the lattice constants of Cu, Ni, and Co surfaces are very close to those of graphene. Besides, according to previous theoretical studies, Cu and Ni/Co represent two typical types of catalysts. Cu has weak interaction with C and does not form carbide phase, while Ni/Co interacts strongly with C and can form stable carbide phase.[10,13,42−45] Therefore, we simulate the growth of graphene on the (111) surfaces of fcc Cu and Ni and the (0001) surface of hcp Co as examples of catalysts for graphene CVD growth in this study.

In this study, a three-layer metal slab with fixed bottom layer atoms was used to represent the metal surface, and then a 6×6 supercell of graphene on the metal surface was used to represent the CVD-grown graphene. The repeated slabs were separated by more than 10 Å to eliminate their interactions between images. Because we were more interested in graphene than substrates, the lattices of metal surfaces were chosen to match the graphene lattice parameters, which lead to small deformation of the substrates (3.75, 1.28, and 1.87% for Cu, Co, and Ni, respectively). The formation energy of a defect in graphene on a metal is defined by

$$E_f = E_{defect} + i\varepsilon_C - E_{M-G} - j\varepsilon_m \quad (1)$$

where E_{defect} and E_{M-G} are the total energies of graphene-metal systems with and without a defect, respectively; ε_C is the energy of one C atom in graphene; ε_m is the energy of a metal atom in bulk, i is 1 for a SV or 2 for a DV, and j is 1 if an extra metal atom is involved in the structure.

In the study of defect formation and healing, an edge of graphene nanoribbon (GNR) was used to represent the growing front of graphene. In previous experimental reports, hexagonal graphene islands with zigzag edges were frequently observed.[46] Recent theoretical study demonstrated the same conclusion by using the kinetic Wulff construction and showed the growth of a zigzag edge mediated by the kink propagation

dx.doi.org/10.1021/ja312687a | J. Am. Chem. Soc. 2013, 135, 4476−4482

with the assistance of a metal atom.[7] Therefore, in the study of defect formation and defect healing, a model of zigzag-edged GNR with a kink on the (111) surface of fcc Cu and Ni with a super cell of 13.47 × 13.47 Å was adopted.

All the calculations in this paper were based on the density functional theory (DFT) and frozen-core all-electron projector-augmented wave method, as implemented in the VASP code.[47] Both generalized gradient approximations (GGA) with Perdew−Burke−Ernzerhof (PBE) exchange−correlation functional including van der Waals (vdW) corrections (DFT-D2 Grimme's method[48] and vdW-DF functional of Langreth and Lundqvist et al.)[49,50] and local density approximation (LDA)[51] were used in the calculation of some typical configurations, and these results are compared in Tables S1 and S2. The configurations calculated by GGA including vdW corrections and LDA method are very similar, but the vacancy formation energies and their diffusion barriers are about 10−15% different. The vacancy formation energies in free-standing graphene calculated by DFT-D2 and vdW-DF methods are almost the same, while the vacancy formation energies in graphene on metal surface calculated by using the vdW-DF method are generally 5−10% larger than those calculated by using the DFT-D2 method. Using the vdW-DF method in the calculation is much more computationally expensive than using the DFT-D2 method. So, to balance the accuracy of the methods and the computational time-consuming, all the data shown in the main text are calculated by the DFT-D2 method.

The energy cutoff for the plane-wave expansion was set to 400 eV. Conjugated gradient (CG) atomic optimization is performed with a criterion of convergence of 0.01 eV/Å. A 2 × 2 **k**-point grid was chosen in the Brillouin zone integration for a 6 × 6 supercell of graphene on the metal surfaces, which can give the results of ∼2% difference with that calculated by more **k**-point sample (see Table S3). The climbing image nudged elastic band method[52] was used to locate the transition states. Spin-polarized DFT was used in all calculations. The scanning tunneling microscope (STM) images are calculated within the Tersoff−Hamann approximation.[53]

3. RESULTS AND DISCUSSION

3.1. Stability and Formation Energies of SV and DV. In free-standing graphene, the removal of a C atom results in three DBs (3DBs) in the sp^2-hybridized honeycomb lattice, while the 3DBs formation is not stable, and two of the C atoms with DBs approach each other to form a five-membered ring (5MR). This leads to the well-known ground structure of SV, being composed of one pentagon and one DB (5DB).[19,22] On the three metal surfaces, such a structure is still stable, but the C atom with a DB bends downward to form a strong C−M bond with a metal atom of the substrate (Figure 1b). Such a SV configuration is very similar to the previously reported SV in graphene on Pt(111) surface.[31] Another stable structure of SV in graphene on metal is the 3DBs formation, in which all three DBs bend downward to one metal atom of the substrate to form three strong C−M bonds, and the metal atom is lifted from the substrate for ∼0.5−0.9 Å (Figure 1c). This configuration is similar to the monovacancy in graphene on Re (0001) surface in a previous report.[32] Considering the high temperature of graphene CVD growth (∼1300 K), active metal atoms may be excited to interact strongly with defects in graphene. Therefore, we introduce a new type of SV structure, called M@3DBs, in which an extra metal atom is drawn from metal bulk to passivate the 3DBs (Figure 1d).

The formation energies for the three types of SV structures on Cu, Ni, and Co surfaces are summarized in Figure 1i. It is clear that all of the formation energies of SV in graphene on metals are significantly smaller than those in free-standing graphene (7.79 eV at the same computational level and 7.4 eV in other theoretical calculation).[19] Among these three SV structures, the 3DBs structure, as shown in Figure 1c, has the lowest formation energy of 4.99, 2.80, and 2.43 eV on Cu, Ni, and Co surfaces, respectively. The formation energies of 3DBs structure were drastically dropped for ∼40, 60, and 70% on Cu, Ni, and Co surfaces, respectively, from 7.79 eV in free-standing graphene. Such a great reduction is attributed to the metal passivation of the DBs. It is notable that, although the M@3DBs formation is more stable than the 5DB structure on the three metal surfaces, it is not the ground structure because there's no enough space in the SV to accommodate the metal atom.

The moiré pattern is characterized as different local stacking configurations between graphene and catalyst surfaces.[54,55] In order to count the effect of moiré pattern of graphene on metal surfaces, three representative configurations of graphene on Cu(111) surface are considered. As shown in Table S4, they are (i) the top fcc, (ii) top hcp, and (iii) hcp−fcc configurations, as those shown in ref 56. The formation energies of SV for fcc and hcp configurations are 4.99 and 4.85 eV, respectively, which is nearly equal because of the exact same stacking order between graphene and the first layer of metal. The SV for configuration (iii) possesses a much higher formation energy of 6.33 eV, which is ∼30% greater than that for fcc or hcp configuration. This is due to the large displacement of the metal atom that is strongly bond to the three C DBs (Table S4). It is worth noting that the models considered in our study are the configurations with low defect formation energy. The packing order of graphene on catalyst surface is an important factor that affects the stability of different defect structures. But considering the large size of the unit cell of the moiré pattern, a complete study on the effect of moiré pattern is extremely computationally expensive and is beyond the scope of this research.

Four different DV structures on metal surfaces, including the known 5|8|5 and 555−777 (Figure 1e,f, respectively) structures, which are well explored in free-standing graphene and carbon nanotubes,[20−22,24] a structure with four DBs (4DBs, Figure 1g) and a structure with one extra metal adatom passivating the four DBs (M@4DBs, Figure 1h) were considered. It was found that the 5|8|5 structure is stable only on the Cu surface. On Ni and Co surfaces, the strong C−M interaction simultaneously breaks the highly strained C−C bonds of the 5|8|5 formation and leads to the 4DBs formation. In the 4DBs structure, a metal atom is drawn up from the metal surface and leaves a vacancy in the catalyst surface, which indicates a strong tendency for the four DBs to be passivated by the metal atom. As shown in Figure 1j, due to the strong interaction between the defective site in graphene and the catalyst surface, the formation energy of 555−777 drops by 0.92, 1.68, and 2.33 eV from that in free-standing graphene on Cu(111), Co(0001), and Ni(111) surfaces, respectively. This indicates the graphene−metal interaction increases in the order of Cu(111) < Co(0001) < Ni(111). For similar reason, the formation energies of another two configurations, 4DBs and M@4DBs, drop in a very similar manner. For all of the three metals considered in this study, the M@4DB DV structures are slightly lower than others, and the formation energies are 5.10 eV on Cu, 3.74 eV on Ni, and 4.31 eV on Co surface, respectively.

dx.doi.org/10.1021/ja312687a | J. Am. Chem. Soc. 2013, 135, 4476−4482

As shown in Figure 1i,j, all of the formation energies for both SV and DV on Cu surface are higher than those on Ni and Co surfaces. This result is expected because Cu−C interaction is known to be weaker than Co−C or Ni−C interaction and Cu cannot passivate the DBs efficiently. For graphene CVD growth, high formation energies imply a potential of synthesizing graphene with a low defect concentration. In this regard, Cu is probably one of the best catalysts for high-quality graphene growth. The formation energy per missing atom (<2.5 eV) of a DV is much lower than that of a SV, that is to say the DV is thermodynamically more favorable than the SV. In order to provide evidence for experimental observation, the simulated STM images for the most stable SV (3DBs) and DV (M@4DBs) structures in graphene on Cu(111) surface at the voltage of −2.0 V are shown in Figure 2 (the most stable SV and DV structures), and others are shown in Figure S1. The simulated STM images for the most stable SV and DV are consistent with a recent experimental work, which has Si and Fe atoms filled in the SV and DV in graphene.[57]

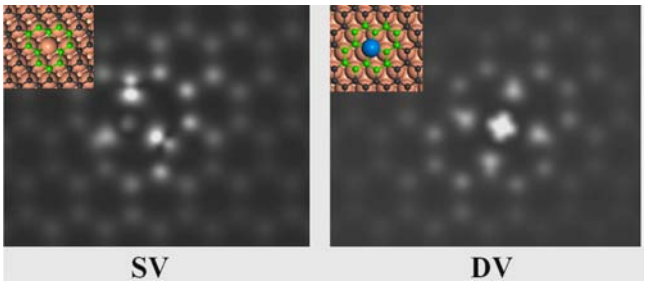

Figure 2. Simulated STM for the most stable SV (3DBs, left) and DV (M@4DBs, right).

3.2. Mobilities of SV and DV. In free-standing graphene or CNTs, the barrier of SV diffusion is very low (1.4 eV according to our calculation, in agreement with the value in literature, 1.3 eV),[19] and thus SV may diffuse very quickly and coalescence into DV or holes[58] or disappear at the edge of the graphene at an elevated temperature. However, in graphene on metal, it shows exceptional stability, which was recently observed in experiments.[31] Here, the diffusion barriers of the most stable SV and DV structures are explored, and the paths of their diffusion on a Cu surface are shown in Figure 3. It is worth noting that the diffusion paths for the SV and DV on Ni and Co are very similar to those on Cu (Figure S2). There's an intermediate state in the diffusion path of the SV, which is similar to the 5DB structure (Figure 1b). The intermediate connects two symmetric 3DBs structures that are separated by a distance of one lattice constant (0.242 nm). The diffusion barrier of a SV on the Cu surface is 2.99 eV, which is much greater than that in free-standing graphene, i.e., 1.4 eV. This is because the metal atom of the substrate sticks to DBs tightly and therefore reduces the mobility of the SV (the metal atom is marked in blue in Figure 3c). Similarly, higher diffusion barriers for SV in Co and Ni surfaces are expected because of the stronger interactions between the metals and DBs. Further calculations confirm the prediction that the diffusion barriers of a SV on Ni and Co surfaces are 3.52 and 3.99 eV, respectively.

The diffusion frequency of SV can be estimated by

$$f = 10^{13} * \exp(-E_D/kT) s^{-1} \quad (2)$$

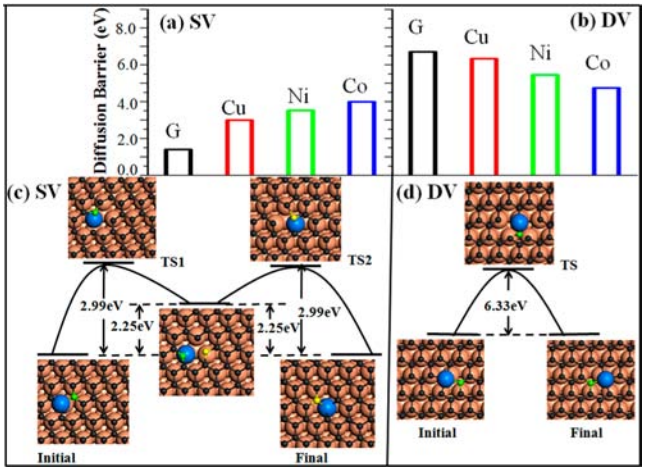

Figure 3. Diffusion barriers of (a) SV and (b) DV in free-standing graphene (G) and graphene on Cu, Ni, and Co surfaces and representative diffusion paths for (c) SV and (d) DV on Cu(111) surface. The moved carbon atoms are colored green and yellow, and the metal adatom is colored blue.

where $kT/h \sim 10^{13}$ s^{-1} and $kT \sim 0.1$ eV at a typical CVD growth temperature ($T \sim 1300$ K), k is the Boltzmann constant, and E_D is the diffusion barrier. Thus, the estimated frequencies on Cu, Ni and Co surfaces are 1, 10^{-3}, and 10^{-5} s^{-1}, respectively. This result indicates that long-distance diffusion of SV on Ni and Co surfaces during CVD growth is almost impossible, while SV may diffuse for certain distances (~10 nm in an hour) on a Cu surface.

The diffusion of M@4DBs, the ground structure of DV, can be regarded as a process of exchanging metal and C atoms (Figure 3d, where the extra metal atom is marked by blue). The calculated DV diffusion barrier energies are 6.33, 5.45, and 4.74 eV on Cu, Ni, and Co surfaces, respectively, which are lower than that in free-standing graphene (~7 eV).[22] But they are still too high to be overcome at the typical CVD growth temperature ($T \sim 1300$ K), and thus we conclude that the DV in graphene on metal surfaces is immobile.

3.3. Formation Processes of DV during CVD Growth. We have shown that DV on all catalyst surfaces is immobile and that only SV on the Cu surface may be able to diffuse for a certain distance. This result indicates that the healing process by the diffusion of vacancies out of a graphene domain, which has a typical size of 1−100 μm, is almost impossible. During the CVD growth of graphene, it is difficult to form a SV with three DBs because the many C atoms around tend to be incorporated into the graphene. In contrast, M@4DBs, the ground structure of DV, which can be regarded as the substitution of two small C atoms by a large metal atom in the graphene lattice, will most probably be formed during growth because the metal atom is involved in the C addition process.[7]

Figure 4a (I and II structures) shows graphene growth on the Cu(111) surface. It presents how a new carbon hexagon was formed nearby a kink of the zigzag edge by the continuous addition of two C atoms onto a kink site at the zigzag edge with the assistant of a Cu atom. When the two C atoms are added from the right side of the metal atom that passivates the kink site, the metal shifts one step left to form a structure which is equivalent to the original one. However, it is also possible to have the metal atom embedded into the graphene lattice when the two C atoms are added from the left (III and IV structures in Figure 4a). As a defect, the structure with the embedded

dx.doi.org/10.1021/ja312687a | J. Am. Chem. Soc. 2013, 135, 4476−4482

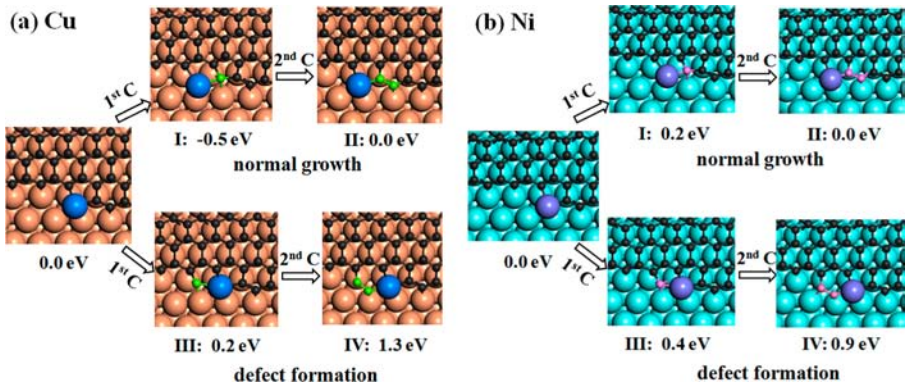

Figure 4. Process of normal growth versus defect formation in graphene on (a) Cu(111) and (b) Ni(111) surfaces (the numbers below the structures are the formation energies).

metal atom has a formation energy which is 1.3 eV higher than the original one. If such a formation was stabilized in the front of graphene growth, the M@4DBs structure of the DV can be formed by further additions of C atoms. Under the condition of near thermal equilibrium at the experimental growth temperature ($kT \sim 0.1$ eV), the concentration of such metal-embedded metal formation can be estimated as

$$C_0 = \exp(-1.3\text{eV}/kT) = 10^{-6} \quad (3)$$

The same formation process of a metal atom embedded structure on Ni(111) surface is shown in Figure 4b. The formation energy of the embedded structure is only 0.9 eV, so the concentration of defects can be estimated to be

$$C_0 = \exp(-0.9\text{eV}/kT) = 10^{-3} \quad (4)$$

It indicates that the concentration of DV in graphene growth on Ni surface is much higher than that on Cu surface. In this regard, Cu is a better catalyst than Ni for high-quality graphene synthesis.

4. FURTHER HEALING OF DV DURING GRAPHENE CVD GROWTH

If the embedded metal atom cannot be healed at the kink, it will stay in the front of growing graphene before the addition of a new hexagon chain. During this period, there is another route for it to be healed, i.e., two C atoms diffuse to the catalyst and draw it out of the front of growth (Figure 5). On a Cu(111) surface, two steps are required to achieve such a healing: (i) the embedded metal atom and the first added C atom form a hexagon on the edge of the graphene; and (ii) the second added C atom replaces the metal and forms a complete front on the edge of graphene. As shown in Figure 5a, step (i) is the threshold step with a barrier of 1.86 eV, and the overall energy drop of the whole process is 4.79 eV, which means the healing is highly exothermic. The healing mechanism can be applied to graphene on a Ni surface as well. As shown in Figure 5b, the threshold step is step (ii) with the corresponding barrier of 2.42 eV, which is higher than that on the Cu surface.

Next, we consider the rate of defect healing during graphene CVD growth by the aforementioned mechanism. Similar to the defect annealing in CNTs,[59] the evolution of the concentration of the embedded metal structure is given by

$$dC = -CK_+dt + (1 - C)K_-dt \quad (5)$$

where C is the concentration of embedded metal atoms, and $K_+ = (k_bT/h) \times \exp(-E^*/k_bT)$ and $K_- = (k_bT/h) \exp[-(E^* + E_r)/k_bT]$ are the reaction constants of the forward and reverse processes whose barriers are E^* and $E^* + E_r$, respectively. Considering the high exothermic reaction, we can neglect the reverse process. Therefore, eq 5 can be simplified to be

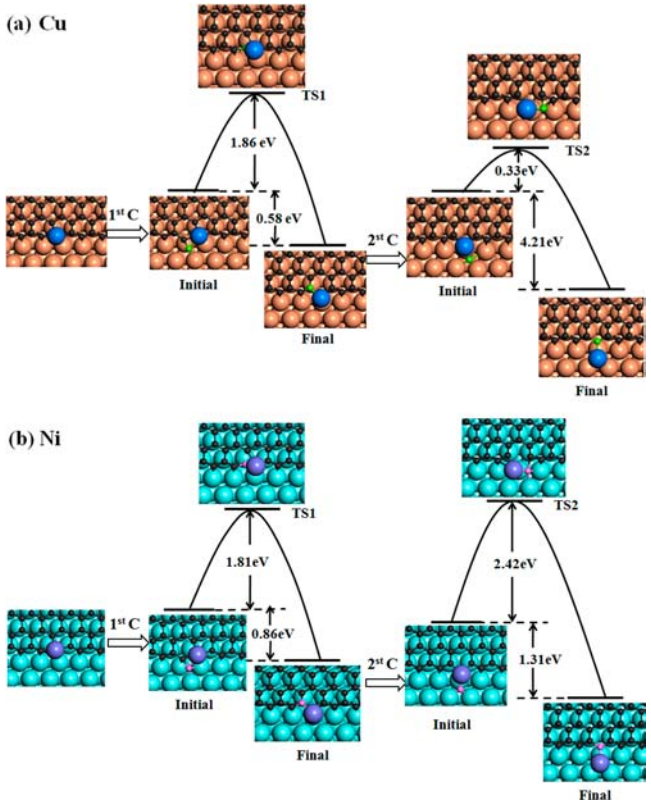

Figure 5. Defect healing process in graphene on (a) Cu(111) and (b) Ni(111) surfaces with two additional carbon atoms.

$$dC = -CK_+dt \quad (6)$$

The solution of eq 6 is

$$C/C_0 = \exp[-t(k_bT/h) \times \exp(-E^*/k_bT)] \quad (7)$$

where C_0 is the initial defect concentration, which can be estimated by eqs 3 and 4. During graphene growth, the addition of each C chain leads to the propagation of growth front for a distance of $\Delta d = 2.13$ Å. So the growth rate is $R = \Delta d/\tau$, where τ is the period for the growth front being filled with a new

dx.doi.org/10.1021/ja312687a | J. Am. Chem. Soc. 2013, 135, 4476−4482

hexagon chain. The reported growth rates are in the range of [0.1, 10^4] nm/s,[60,61] and thus τ is in the range of [1, 10^5] s.

Figure 6 shows the rate of DV healing as a function of growth rate R at different temperatures on a Cu or Ni surface. The

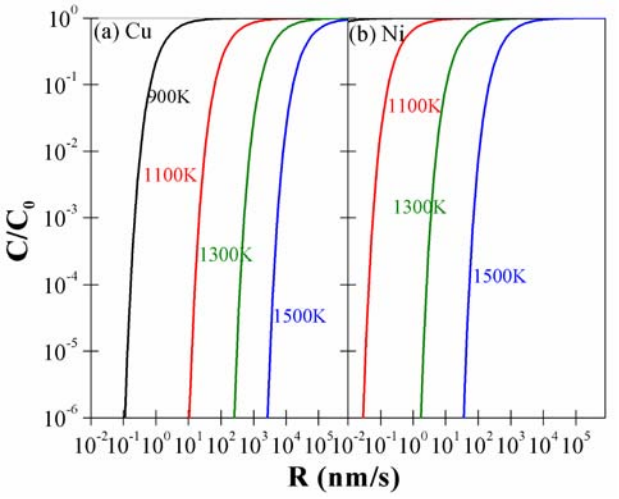

Figure 6. Rate of point defect healing in graphene CVD growth on (a) Cu(111) and (b) Ni(111) surfaces as functions of graphene growth rate R at different temperatures.

difference in the defect healing on Cu and Ni is clearly shown. For example, at the temperature of 1300 K and the growth rate of 10−100 nm/s, the healing rate is greater than 99.999% on Cu but only 90% or less on Ni. This result can clearly explain why 1300 K is the typical experimental temperature for graphene CVD growth on Cu surfaces.[40,50] It also shows that both the temperature and the growth rate play crucial roles in the defect healing. The faster growth at lower temperature leads to a higher defect concentration, and slower growth at higher temperature results in a lower concentration. The temperature-dependent defect healing is in consistent with the report of Jacobson et al., in which high-quality graphene is obtained by high-temperature annealing.[30] More importantly, we find that the defect healing exhibits higher efficiency on Cu than on Ni surfaces, which can also prove that Cu can be a better catalyst for graphene CVD growth from a new aspect. Besides, the M@4DBs structure may have other important applications. The embedded metal atom can be used as a catalyst for various chemical reactions.[62−64] Therefore, this study also shows a route of synthesizing graphene embedded with various catalysts.

5. CONCLUSIONS

In summary, we have performed a comprehensive theoretical investigation on the formation, mobility, and healing of SV and DV in graphene on metal surfaces, including Cu, Ni, and Co. It was shown that, due to the passivation of active C atoms of the defects by metal atoms, the formation energies of both SV and DV are greatly reduced and that the diffusion barriers of SV are greatly increased compared to those in free-standing graphene. The most stable SV and DV structures tend to have more DBs passivated by a metal atom instead of forming topological defects, such as five-, seven-, and eight-membered rings. Being different from those in free-standing graphene, the SV on metals is no longer mobile. Furthermore, the kinetics of DV formation and their healing during graphene CVD growth were considered. Our calculations show that, at the typical condition of graphene CVD growth (1300 K with the growth rate of 10−100 nm), the concentration of defects on a Cu surface can be greatly reduced to $10^{-6} * 10^{-6} = 10^{-12}$ or lower. However, on a Ni surface, higher concentration of DV can be observed during CVD growth. This study indicates that those metals which have weak interaction with carbon (e.g., Au, Ag, Cu, etc) are better catalysts for high-quality graphene growth than those that interact strongly with carbon (e.g., Ni, Co, Fe, Pt, Ru, Rh, etc). On the other hand, those metals which interact strongly with carbon can be used in synthesizing new types of graphene embedded with metal atoms, which can serve as efficient catalyst for various chemical reactions.

■ ASSOCIATED CONTENT

Supporting Information

Comparison of configurations, formation energies and diffusion barriers of vacancies in free-standing graphene and on Cu(111) surface by DFT-D2, vdW-DF and LDA methods are presented in Tables S1 and S2; tests for different **k**-point grids for a 6 × 6 supercell of graphene on Cu surface are presented in Table S3; configurations and formation energies of SV in graphene on Cu(111) surface with different positions of C and Cu atoms are shown in Table S4; simulated STM images for SV and DV in graphene on Cu(111) surfaces and diffusion path and barrier energies of DV on Ni(111) and Co(0001) surfaces are presented in Figures S1 and S2, respectively. This material is available free of charge via the Internet at http://pubs.acs.org.

■ AUTHOR INFORMATION

Corresponding Author

feng.ding@polyu.edu.hk; apafyan@polyu.edu.hk

Notes

The authors declare no competing financial interest.

■ ACKNOWLEDGMENTS

This work was supported by the Postdoctoral Fellowship Scheme (G-YX4R) in Hong Kong Polytechnic University.

■ REFERENCES

(1) Dimiev, A.; Kosynkin, D. V.; Sinitskii, A.; Slesarev, A.; Sun, Z.; Tour, J. M. *Science* **2011**, *331*, 1168.
(2) Geim, A. K. *Science* **2009**, *324*, 1530.
(3) Geim, A. K.; Novoselov, K. S. *Nat. Mater.* **2007**, *6*, 183.
(4) Chen, J.-H.; Jang, C.; Xiao, S.; Ishigami, M.; Fuhrer, M. S. *Nat. Nano* **2008**, *3*, 206.
(5) Cao, H.; Yu, Q.; Colby, R.; Pandey, D.; Park, C. S.; Lian, J.; Zemlyanov, D.; Childres, I.; Drachev, V.; Stach, E. A.; Hussain, M.; Li, H.; Pei, S. S.; Chen, Y. P. *J. Appl. Phys.* **2010**, *107*, 044310.
(6) Cao, H.; Yu, Q.; Jauregui, L. A.; Tian, J.; Wu, W.; Liu, Z.; Jalilian, R.; Benjamin, D. K.; Jiang, Z.; Bao, J.; Pei, S. S.; Chen, Y. P. *Appl. Phys. Lett.* **2010**, *96*, 122106.
(7) Shu, H.; Chen, X.; Tao, X.; Ding, F. *ACS Nano* **2012**, *6*, 3243.
(8) Yuan, Q.; Hu, H.; Gao, J.; Ding, F.; Liu, Z.; Yakobson, B. I. *J. Am. Chem. Soc.* **2011**, *133*, 16072.
(9) Gao, J.; Yip, J.; Zhao, J.; Yakobson, B. I.; Ding, F. *J. Am. Chem. Soc.* **2011**, *133*, 5009.
(10) Yuan, Q.; Gao, J.; Shu, H.; Zhao, J.; Chen, X.; Ding, F. *J. Am. Chem. Soc.* **2012**, *134*, 2970.
(11) Zhang, W.; Wu, P.; Li, Z.; Yang, J. *J. Phys. Chem. C* **2011**, *115*, 17782.
(12) Li, Z.; Wu, P.; Wang, C.; Fan, X.; Zhang, W.; Zhai, X.; Zeng, C.; Li, Z.; Yang, J.; Hou, J. *ACS Nano* **2011**, *5*, 3385.

(13) Li, X.; Magnuson, C. W.; Venugopal, A.; An, J.; Suk, J. W.; Han, B.; Borysiak, M.; Cai, W.; Velamakanni, A.; Zhu, Y.; Fu, L.; Vogel, E. M.; Voelkl, E.; Colombo, L.; Ruoff, R. S. *Nano Lett.* **2010**, *10*, 4328.
(14) Novoselov, K. S.; Geim, A. K.; Morozov, S. V.; Jiang, D.; Zhang, Y.; Dubonos, S. V.; Grigorieva, I. V.; Firsov, A. A. *Science* **2004**, *306*, 666.
(15) Yu, Q.; et al. *Nat. Mater.* **2011**, *10*, 443.
(16) Li, X.; Magnuson, C. W.; Venugopal, A.; Tromp, R. M.; Hannon, J. B.; Vogel, E. M.; Colombo, L.; Ruoff, R. S. *J. Am. Chem. Soc.* **2011**, *133*, 2816.
(17) Hernandez, Y.; et al. *Nat. Nano* **2008**, *3*, 563.
(18) Krasheninnikov, A. V.; Lehtinen, P. O.; Foster, A. S.; Nieminen, R. M. *Chem. Phys. Lett.* **2006**, *418*, 132.
(19) El-Barbary, A. A.; Telling, R. H.; Ewels, C. P.; Heggie, M. I.; Briddon, P. R. *Phys. Rev. B* **2003**, *68*, 144107.
(20) Lee, G.-D.; Wang, C. Z.; Yoon, E.; Hwang, N.-M.; Kim, D.-Y.; Ho, K. M. *Phys. Rev. Lett.* **2005**, *95*, 205501.
(21) Lee, G.-D.; Wang, C. Z.; Yoon, E.; Hwang, N.-M.; Ho, K. M. *Phys. Rev. B* **2006**, *74*, 245411.
(22) Banhart, F.; Kotakoski, J.; Krasheninnikov, A. V. *ACS Nano* **2011**, *5*, 26.
(23) Lee, G.-D.; Wang, C. Z.; Yoon, E.; Hwang, N.-M.; Ho, K. M. *Appl. Phys. Lett.* **2008**, *92*, 043104.
(24) Kotakoski, J.; Krasheninnikov, A. V.; Nordlund, K. *Phys. Rev. B* **2006**, *74*, 245420.
(25) Lee, G.-D.; Wang, C.-Z.; Yoon, E.; Hwang, N.-M.; Ho, K.-M. *Appl. Phys. Lett.* **2010**, *97*, 093106.
(26) Krasheninnikov, A. V.; Lehtinen, P. O.; Foster, A. S.; Pyykko, P.; Nieminen, R. M. *Phys. Rev. Lett.* **2009**, *102*, 126807.
(27) Krasheninnikov, A. V.; Nieminen, R. M. *Theor. Chem. Acc.* **2011**, *129*, 625.
(28) Lee, D. H.; Lee, W. J.; Lee, W. J.; Kim, S. O.; Kim, Y.-H. *Phys. Rev. Lett.* **2011**, *106*, 175502.
(29) Santos, E. J. G.; Sanchez-Portal, D.; Ayuela, A. *Phys. Rev. B* **2010**, *81*, 125433.
(30) Jacobson, P.; Stoger, B.; Garhofer, A.; Parkinson, G. S.; Schmid, M.; Caudillo, R.; Mittendorfer, F.; Redinger, J.; Diebold, U. *J. Phys. Chem. Lett.* **2012**, *3*, 136.
(31) Ugeda, M. M.; Fernandez-Torre, D.; Brihuega, I.; Pou, P.; Martinez-Galera, A. J.; Perez, R.; Gomez-Rodriguez, J. M. *Phys. Rev. Lett.* **2011**, *107*, 116803.
(32) Miniussi, E.; Pozzo, M.; Baraldi, A.; Vesselli, E.; Zhan, R. R.; Comelli, G.; Mente, T. O.; Nio, M. A.; Locatelli, A.; Lizzit, S.; Alfe, D. *Phys. Rev. Lett.* **2010**, *106*, 216101.
(33) Preobrajenski, A. B.; Ng, M. L.; Vinogradov, A. S.; Martensson, N. *Phys. Rev. B* **2008**, *78*, 073401.
(34) Marchini, S.; Gunther, S.; Wintterlin, J. *Phys. Rev. B* **2007**, *76*, 075429.
(35) Zhang, Y.; Gomez, L.; Ishikawa, F. N.; Madaria, A.; Ryu, K.; Wang, C.; Badmaev, A.; Zhou, C. *J. Phys. Chem. Lett.* **2010**, *1*, 3101.
(36) Lee, Y.; Bae, S.; Jang, H.; Jang, S.; Zhu, S.-E.; Sim, S. H.; Song, Y. I.; Hong, B. H.; Ahn, J.-H. *Nano Lett.* **2010**, *10*, 490.
(37) N'Diaye, A. T.; Bleikamp, S.; Feibelman, P. J.; Michely, T. *Phys. Rev. Lett.* **2006**, *97*, 215501.
(38) Sutter, P.; Sadowski, J. T.; Sutter, E. *Phys. Rev. B* **2009**, *80*, 245411.
(39) Kwon, S.-Y.; Ciobanu, C. V.; Petrova, V.; Shenoy, V. B.; Bareno, J.; Gambin, V.; Petrov, I.; Kodambaka, S. *Nano Letts* **2009**, *9*, 3985.
(40) Reddy, K. M.; Gledhill, A. D.; Chen, C.-H.; Drexler, J. M.; Padture, N. P. *Appl. Phys. Lett.* **2011**, *98*, 113117.
(41) Varykhalov, A.; Rader, O. *Phys. Rev. B* **2009**, *80*, 035437.
(42) Li, X.; Cai, W.; Colombo, L.; Ruoff, R. S. *Nano Lett.* **2009**, *9*, 4268.
(43) Lahiri, J.; Miller, T. S.; Ross, A. J.; Adamska, L.; Oleynik, I. I.; Batzill, M. *New J. Phys.* **2011**, *13*, 025001.
(44) Gao, J.; Yuan, Q.; Hu, H.; Zhao, J.; Ding, F. *J. Phys. Chem. C* **2011**, *115*, 17695.
(45) Chen, H.; Zhu, W.; Zhang, Z. *Phys. Rev. Lett.* **2010**, *104*, 186101.
(46) Tian, J.; Cao, H.; Wu, W.; Yu, Q.; Chen, Y. P. *Nano Lett.* **2011**, *11*, 3663.
(47) Kresse, G.; Furthmuller, J. *Phys. Rev. B* **1996**, *54*, 11169.
(48) Grimme, S. *J. Comput. Chem.* **2006**, *27*, 1787.
(49) Dion, M.; Rydberg, H.; Schröder, E.; Langreth, D. C.; Lundqvist, B. I. *Phys. Rev. Lett.* **2004**, *92*, 246401.
(50) Klimeš, J.; Bowler, D. R.; Michaelides, A. *Phys. Rev. B* **2011**, *83*, 195131.
(51) Kresse, G.; Joubert, D. *Phys. Rev. B* **1999**, *59*, 1758.
(52) Henkelman, G.; Uberuaga, B. P.; Jónsson, H. *J. Chem. Phys.* **2000**, *113*, 9901.
(53) Tersoff, J.; Hamann, D. R. *Phys. Rev. Lett.* **1983**, *50*, 1998.
(54) Gao, L.; Guest, J. R.; Guisinger, N. P. *Nano Lett.* **2010**, *10*, 3512.
(55) Chen, X.; Liu, S.; Liu, L.; Liu, X.; Liu, X.; Wang, L. *Appl. Phys. Lett.* **2012**, *100*, 163106.
(56) Zhao, W.; Kozlov, S. M.; Hofert, O.; Gotterbarm, K.; Lorenz, M. P. A.; Vines, F.; Papp, C.; Gorling, A.; Steinruck, H.-P. *J. Phys. Chem. Lett.* **2011**, *2*, 759.
(57) Chisholm, M. F.; Duscher, G.; Windl, W. *Nano Lett.* **2012**, *12*, 4651.
(58) Huang, J. Y.; Ding, F.; Yakobson, B. I. *Phys. Rev. B* **2008**, *78*, 155436.
(59) Yuan, Q.; Xu, Z.; Yakobson, B. I.; Ding, F. *Phys. Rev. Lett.* **2012**, *108*, 245505.
(60) Wu, B.; Geng, D.; Guo, Y.; Huang, L.; Xue, Y.; Zheng, J.; Chen, J.; Yu, G.; Liu, Y.; Jiang, L.; Hu, W. *Adv. Mater.* **2011**, *23*, 3522.
(61) Robertson, A. W.; Warner, J. H. *Nano Lett.* **2011**, *11*, 1182.
(62) Yoo, E.; Okata, T.; Akita, T.; Kohyama, M.; Nakamura, J.; Honma, I. *Nano Lett.* **2009**, *9*, 2255.
(63) Lu, Y.-H.; Zhou, M.; Zhang, C.; Feng, Y.-P. *J. Phys. Chem. C* **2009**, *113*, 20156.
(64) Li, F.; Zhao, J.; Chen, Z. *J. Phys. Chem. C* **2012**, *116*, 2507.